A Two-Stage Marked Point-Process Model for Multi-Subject FMRI Data

Adél Lee Aila Särkkä Tara M. Madhyastha

September 22, 2015

Functional Magnetic Resonance Imaging (fMRI) is a neuroimaging technique that helps us to understand the relationship between neural activation and mental activities, such as perception or motor processing tasks. During an fMRI session a series of three dimensional images of the brain is acquired at regular intervals over a period of about 3 to 5 minutes. The series of images acquired during a session reflects the blood oxygenation-level dependent (BOLD) responses in the brain resulting from neural activity. The BOLD response arises from oxygenation changes in the capillary network surrounding activated neurons.

To identify areas of activation in the brain, it is common to fit a linear model to the time series recorded for each voxel in the three-dimensional brain volume. The resulting voxel-wise estimates of activation are then analysed spatially to identify brain regions that are involved in specific tasks.

Multi-subject fMRI studies are often used in fMRI to gain insight into the relationship between task and neural activation for different groups or populations of individuals. A question that has received much attention in the literature is how to combine information about activation across individuals. A standard approach in the fMRI literature has been to fit a linear mixed effects model to the multi-subject time-series data recorded at each voxel location [Beckmann et al., 2003, Friston et al., 2002a,b, Nichols and Holmes, 2002, Woolrich et al., 2004, Worsley et al., 2002].

One of the main shortcomings of this voxel-by-voxel (or 'low-level') analysis approach is that the spatial structure of the BOLD response is not accounted for. The BOLD signal arises from oxygenation changes in the capillaries surrounding the site of neural activity, as well as in larger veins that drain the activated tissue area. As a result the BOLD response is often spread over a neighbourhood of several voxels. These characteristics of the BOLD response are recognized in high-level imaging models [Kim et al., 2010, Kang et al., 2011, Xu et al., 2009, Hartvig, 2002, Weeda et al., 2009] that capture the location, shape and size of the BOLD response.

Some authors specifically considered how high-level models can be used to combine information about activation across subjects. Kang et al. [2011] proposed an hierarchical spatial point process model that assumes that the foci (or locations) of activation that they identify for each subject are the offspring of a latent population process. The authors are specifically interested in inference on the locations of population centers. Kim et al. [2010], on the other hand, used a nonparametric approach. The authors assume that there is a true underlying image template and that the individual subject patterns of activation are noisy realization of the true template. Xu et al. [2009] developed a Bayesian hierchical mixture model approach. The authors were also interested in identifying population centers of activation and in modeling the variation of the individual centers around population centers.

In this paper, we also use high level statistical image analysis methods to identify the

image elements of interested (which we refer to as activation units or centers). Our approach is based on using a marked spatial point process prior to identify the activation units for each subject [Baddeley and Lieshout, 1993, Al-Awadhi et al., 2011]. Rather than using these units to identify latent population centers of activation, we are interested in understanding the interaction between these units across subjects.

We develop a two-stage model. In the first stage we identify a set of activation units for each subject. These units summarize the location, height and size (spatial extent) of activation for each subject. In our second stage analysis, we assume that activation locations that are spatially close in the brain volume result from the same functional area. Based on this assumption, we developed a pairwise interaction point process model that consider inter-subject points that are spatially close to be neighbors. We use this model to study the type and strength of inter-subject interaction patterns observed in different functional regions of the brain.

The model that we develop in this paper is motivated by the unique features of multi-subject fMRI data. In the spatial point process literature there are several examples of analyzing replicated data (data collected from different individuals under the same experimental conditions or for at different locations within the same environment) [Myllymäki et al., 2012, Waller et al., 2011, Schladitz et al., 2003, Diggle et al., 2000], and also of using point process models to study interactions between different types of points on the same image [Eckel et al., 2009, Diggle et al., 2006]. In this paper, we also consider point patterns replicated under the same experimental conditions and multitype data. However, our data has the additional feature that the point pattern identified for each subject share spatial information (*i.e.* the subject images have been spatially aligned so that a specific voxel location matches to the same functional area in the brain). With this features in mind, we developed a model that gives us insight into how information about activation is shared across subjects in different functional regions of the brain.

We use a Bayesian framework to identify the activation centers and study their inter-subject interactions. In both stages of the model we use Markov chain Monte Carlo methods to simulate realizations from the posterior.

Our paper is organized as follows. In Section 1 we describe the data set used in our analysis, and in Sections 2 and 3 we specify the First and Second Stage models, respectively. This is followed by a description of our MCMC algorithm in Section 4. We fit our model to an fMRI data set in Section 5 and end with a discussion of our results in Section 6.

1 fMRI data

The model that we develop in this paper is motivated by multi-subject fMRI studies. We use data from a multi-subject study conducted by the Integrated Brain Imaging Center at the University of Washington. This study includes a group of 21 control individuals (9 males) with an average age of 62 (standard deviation 10). The subjects performed an attention network test [Fan et al., 2005], which consists of three cue conditions and two target conditions.

Here we consider activation corresponding to the target conditions only. The target conditions consisted of five visually presented arrows (arranged horizontally in one line). The central arrow (or target) either pointed in the same direction as the four flanking arrows (congruent target) or in the opposite direction (incongruent target) as the four flanking arrows. The participant had to identify the direction of the target arrow by pressing a button with the left index finger if the central arrow pointed leftward or by pressing a button with the right index finger if the arrow pointed rightward.

The target conditions were designed to help isolate the executive control network in the brain. Here we explore the brain areas involved in both target conditions. For a detailed description of the characteristics of the study participants, the attention network test, MRI acquisition and pre-processing, consult Madhyastha et al. [2015].

After pre-processing the brain volume data obtained for each subject, a general linear model was fitted to the time-series at each voxel location using the brain imaging software, FSL's [Jenkinson et al., 2012] FMRI Expert Analysis Tool (FEAT) version 6.0. Note that the time-series data was not combined across subjects (*i.e.*, a seperate linear model was fitted for each subject). The regression coefficient estimates representing the target condition were then transformed into z-statistics[1]. The resulting volumes of z-statistics (one volume per subject) are then analyzed to identify regions of activation.

We select an axial slice that runs through the inferior lateral occipital cortex, the frontal operculum cortex and insular cortex for our analysis. The lateral occipital cortex is on the visual pathway, visually processing the target. The motor network needs to be activated to press a button, and to do that the insula is part of a salience network that helps to recruit other regions in support of motor function.

By selecting a slice, we identify 21 maps (sets of z-statistics) that are used as input for our first stage model. We only consider areas with positive z-values for this analysis. Therefore, voxels with z-values less than 0 are assigned a value of 0. We display the map of z-statistics for four of the subjects in our dataset in Figure 1. Note the variability in height and size of activation among the subjects.

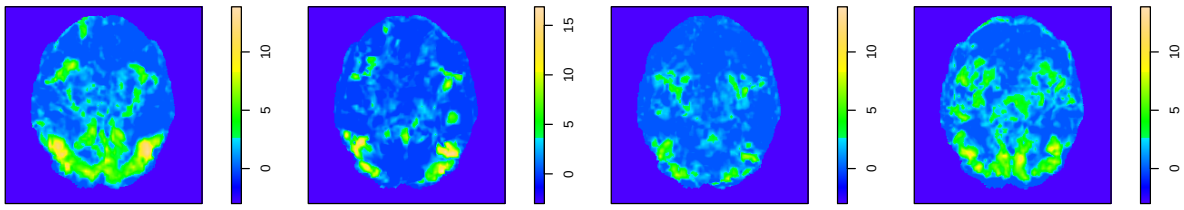

Figure 1: The activation surfaces (maps of z-statistics) of four of the subjects for the selected axial slice.

2 Model Specification: First Stage Model

As mentioned above, we develop a two-stage model in this paper. In the first stage model, we use the activation images (spatial maps of z-statistics) as input and identify the image elements of interest. These elements (or 'activation units' or 'centers' capture the features of the BOLD responses that we expect to see in areas of activation. In particular, we are looking for spatially extended areas that are smooth and that show a higher level of activation than what we expect to see under the null hypothesis of no activation in the brain volume. Each activation unit is described in terms of its location, height (strength of activation), and size (spatial extent of

[1]This involves calculating the probability of observing a value less than or equal to the coefficient estimate under the relevant distribution. The calculated probability is then transformed into the corresponding z-statistic under the standard normal distribution.

activation). By identifying the activation units, we can summarize the activation surface of each subject using relatively few parameters.

2.1 Likelihood

We denote the activation surface observed for subject s by the set of intensity measurements $Y_s = \{y_{s,v} | v \in V\}$. Here V is the two-dimensional grid on which the data is observed.

We model the observed data (image) for subject s as the sum of an underlying activation pattern and a noise term,

$$y_{s,v} = A(v; x_s) + \eta_{s,v}, \qquad \eta_{s,v} \sim \mathcal{N}(0, \tau^2),$$

for $s = 1, \ldots, S$ and $v \in V$. We assume that the noise $\eta_{s,v}$ is independently distributed across the grid and the subjects.

The *activation surface* $A_s = \{A(v; x_s) | v \in V\}$ for subject s is a deterministic function, given the configuration of marked points $\boldsymbol{x}_s = \{x_{s,1}, \ldots, x_{s,n_s}\}$ for subject s.

$$A(v; \boldsymbol{x}_s) = h(v; x_{s,1}) + \cdots + h(v; x_{s,n_s}), \tag{1}$$

for $v \in V$. We refer to each marked point $x_{s,j} = (\mu_{s,j}, a_{s,j}, d_{s,j})$ as an *activation unit*. These units summarise the location μ, height a and size d of activation.

The function $h(v; x_{s,j})$ is a Gaussian bell. The functional form of each bell is $h(v; (\mu_{s,j}, a_{s,j}, d_{s,j})) = a_{s,j} d_{s,j} f_{s,j}(v)/\log 2$ where $f_{s,j}(v) = f(v; \mu_{s,j}, \Sigma_{s,j})$ is the multivariate normal density function with mean $\mu_{s,j}$ and covariance matrix $\Sigma_{s,j}$,

$$\Sigma_{s,j} = \frac{d_{s,j}}{2\pi \log 2} I.$$

This specification of the covariance matrix, where I is a two-dimensional identity matrix, implies that we only consider circular bells. In this context, a is interpreted as the maximum height of the Gaussian bell, *i.e.* $h(\mu_{s,j}; (\mu_{s,j}, a_{s,j}, d_{s,j})) = a_{s,j}$, and d is the area of the cross section of the Gaussian bell at half of the maximum height. The cross section of the bell is taken so that it is parallel to the level of the grid, implying that the cross section is a circle with area d.

2.2 Prior model for the configuration of activation units

We require a prior model that will allow us to identify the underlying units of activation for each subject. In this section we define a marked spatial point process prior that will allow us to pick up the true activation signal in the data by enforcing a minimal set of constraints.

In this analysis, we assume that the marks are independent of the locations and also that the two marks (height and size) are independent of each other.

Note that we will indicate a realisation of the marked spatial point-process prior defined in this section as $\boldsymbol{x} = \{\boldsymbol{x}_1, \ldots, \boldsymbol{x}_S\}$, where $\boldsymbol{x}_s = \{x_{s,1}, \ldots, x_{s,n_s}\}$. In this analysis the number of subjects S is fixed, but the number of activation centres for each subject, n_s, is random.

Location of activation

We define a hard-core prior on the location points of each subject,

$$p(\mu_{s,1}, \ldots, \mu_{s,n_s}) = \begin{cases} \prod_{j=1}^{n_s} \beta(\mu_{s,j}) & \text{if } \|\mu_{s,j} - \mu_{s,j'}\| > R_W \quad \forall j \neq j', \\ 0 & \text{otherwise,} \end{cases} \tag{2}$$

for $s = 1, \ldots, S$.

This prior specification is motivated by our understanding of the BOLD response. As mentioned above, the BOLD signal arises from oxygenation changes in the capillaries surrounding the site of neural activity. In order to identify separate, non-overlapping areas of activation, we enforce a minimal distance, R_W, that our location points should be apart within subjects. We set R_W based on an exploratory analysis of the data. This is dicussed in Section 2.3.

The first order term β can be modeled as a function of a covariate Z that reflects how the intensity of the point pattern is expected to change across the brain. However, we want the data Y to determine the intensity of the activation units across the grid V in the first stage model. As a result, we set $\beta = 1$.

We also note that the prior models the locations parameters to be independent across subjects. As with the intensity function, we do not assume that the locations are independent across subjects (and will explicitely model these interactions in the second stage analysis), but we want the data Y to determine the locations of activation centers in the first stage analysis[2].

Height and size of activation units

In order to find spatially extended areas where the z-statistics have high values, *i.e.* areas where BOLD responses occur, we need to consider carefully how to specify the prior on the height and size parameters.

The prior on the height, p_a, is chosen so that lower values of a are penalised. We choose an inverse-gamma prior for a, $a \sim \text{Inv-gam}(\alpha_a, \beta_a)$, $a \in (0, C_a]$, with probability density function

$$p_a(a) \propto a^{-(\alpha_a+1)} \exp(-1/(a\beta_a)). \tag{3}$$

This distribution gives us control over penalising smaller values of a through adjusting α_a and β_a. Also note that the prior is truncated to the interval $(0, C_a]$. This is only a practical constraint that is helpful when implementing the model. (We always set C_a to exceed the maximum intensity, *i.e.* $C_a > \max\{y_v : v \in V\}$.)

It is also important to choose the prior for the size d carefully. We specify an uniform prior for the size, $d \sim \text{Unif}(d_{low}, d_{up})$, for $d \in [d_{low}, d_{up}]$. The challenge is to scale the interval $[d_{low}, d_{up}]$ accurately so that the size of detected activation centres corresponds to the spatial scale of the BOLD response.

2.3 Setting model parameters and hyperparameters

Here we describe the methods used to specify the model parameter τ^2 and the hyperparameters R_W, α_a, β_a, C_a, d_{low}, d_{up}.

To specify the variance of the likelihood model, τ^2, we recall that under the null hypothesis of no activation in the brain volume the z-statistics in the map should behave like samples from the standard normal distribution. In order to identify areas where the z-statistics deviate from this behavior, we set $\tau^2 = 1$.

[2]We did consider a first stage model that allows for between-subject interactions in locations. In particular, we used a Geyer saturation model to specify between-subject interaction. However, we found that this model encourages too many activation units to be picked up, especially activation units with low height and small size (*i.e.* units that seem to resemble noise and rather than signal). We decided to remove the between-subject component from the model because it enforces too strong a prior and makes it difficult to pick up the true signal.

To get insight into setting the hyperparameters, we did an exploratory analysis of the activation surfaces of the 21 subjects. This was done by smoothing the activation surface of each subject and identifying the local maxima of the smoothed surfaces. (Smoothing was implemented by convolving each functional image with a fixed-width Gaussian filter.) To specify R_W, we explored the nearest-neighbor within-subject distances between the local maxima. We found that all nearest neighbor maxima were at least 5 voxels apart (within subjects). Based on this, we set the within-subject hardcore distance R_W to be equal to 5mm[3].

The hyperparameters d_{low} and d_{up} specify the interval over which the size of activation centres can range. Recall that the size d is the area of the circle that is the cross-section of an activation centre (Gaussian bell) at half its height. We have to keep in mind that the BOLD signal often extends beyond the capillary network adjacent to the activated neurons. For this reason, we allow neighbouring activation centres to overlap. We constrain the overlap so that the diameter of the circle at half height corresponding to d_{up} is 2 times the hardcore distance R_W, *i.e.* the diameter of d_{low} is set to correspond to a distance of 10 voxels. We set d_{low} so that our model can detect sharp, localised peaks of activation. We let the diameter corresponding to d_{low} be equal to a distance of 5 voxels (*i.e.* $d_{low} = 20\text{mm}^2$ and $d_{up} = 80\text{mm}^2$).

In Section 2.2 we specified an inverse-gamma prior on a with hyperparameters α_a and β_a. We need to specify α_a and β_a so that our model pick up spatially extended areas with high z-values. To achieve this, we fitted our model to our fMRI data for different settings of α_a and β_a. We found that for $\alpha_a = 10$ and $\beta_a = 0.023$, all fitted activation centres have a height of at least 1 and more than 75% have a height of at least 2. We used these settings.

2.4 Posterior distribution

The posterior density function of the first stage model is

$$p(\boldsymbol{x}|Y) \propto \begin{cases} \exp\{-\frac{1}{2\tau^2}\sum_{s=1}^{S}\sum_{v\in V}(y_{s,v} - A(v;\boldsymbol{x}_s))^2\}\times & \\ \quad \prod_{s=1}^{S}\prod_{j=1}^{n_s} p_a(a_{s,j})p_d(d_{s,j}) & \text{if } \|\mu_{s,j} - \mu_{s,j'}\| > R_W \quad \forall j \neq j', \\ 0 & \text{otherwise} \end{cases}$$

3 Second Stage Model

As input to the second stage model we use the location points $\boldsymbol{\mu}$ that correspond to the configuration of activation units $\boldsymbol{x}$ that maximized the posterior $p(\boldsymbol{x}|Y)$. We consider the point pattern $\boldsymbol{\mu}$ to be a multitype process for which each subject is a different type. The subscript s is used to distinguish between subjects (or types), with $\boldsymbol{\mu}_s = \{\mu_{s1}, \ldots, \mu_{sn_s}\}$ denoting the set of location points for subject s.

We fit a pairwise interaction model to the point pattern data $\boldsymbol{\mu}$. Pairwise interaction point process models are typically suitable for modeling regularity but not clustering. Various models have been proposed in literature to overcome this limitation, e.g. area-interaction point processes [Baddeley and Van Lieshout, 1995], continuous random cluster Markov point processes [Møller, 1999], and interacting neighbor processes [Grabarnik and Särkkä, 2001]. For our application, we are looking for a parsiminious model that can model clustered patterns and that can easily be extended to handle multitype data. We found that the Geyer's saturation model [Geyer, 1999] fit these criteria well.

The Geyer saturation process model for univariate data has a density function of the form

$$f(\boldsymbol{\mu}) = k\beta^n\gamma^{s(\boldsymbol{\mu})} \tag{4}$$

[3]The voxel dimension for the data that we analyze in this paper is $1 \times 1 \times 1$mm.

where k denotes the normalizing constant, β the intensity parameter, n is the number of points, and γ is the interaction parameter. Here $s(\boldsymbol{\mu})$ is the sum of the number of neighbors of each point,

$$\begin{aligned} s(\boldsymbol{\mu}) &= \sum_{j=1}^{n} \min(d, \sum_{j' \neq j} \mathbf{1}[\|\mu_j - \mu_{j'}\| \leq R]) \\ &= \sum_{j=1}^{n} \min(d, N_{\boldsymbol{\mu}_{-j}}(\mu_j)). \end{aligned}$$

Here d is the saturation threshold and $N_{\boldsymbol{\mu}_{-j}}(\mu_j)$ is the number of neighbors that the point μ_j has in the set of points $\boldsymbol{\mu}_{-j} = \{\mu_1, \ldots, \mu_{j-1}, \mu_{j+1}, \ldots, \mu_n\}$. Here we define two points to be neighbors if they are less or equal to a distance of R apart. For $\gamma = 1$ the process becomes the Poisson process, for $\gamma < 1$ the density (4) models repulsion, and for $\gamma > 1$ clustering.

We extend the univariate Geyer model to model multitype processes. Here we consider each individual to be a type. Our interest is in understanding the between-subject patterns in activation and we, therefore, propose the following model:

$$p(\boldsymbol{\mu}) = \begin{cases} k\beta(\boldsymbol{\mu}) \times \gamma_B^{S_B(\boldsymbol{\mu})} & \text{if } \|\mu_{s,j} - \mu_{s,j'}\| > R_W \quad \forall s \text{ and } j \neq j', \\ 0 & \text{otherwise.} \end{cases} \tag{5}$$

As before, k denotes the normalizing constant, β the intensity function, and γ_B is the interaction parameter. Here the total number of between-subject neighbors are given by

$$\begin{aligned} s_B(\boldsymbol{\mu}) &= \sum_{s=1}^{S} \sum_{j=1}^{n_s} \min(d, \sum_{s' \neq s} \sum_{j'=1}^{n_{s'}} \mathbf{1}[\|\mu_{sj} - \mu_{s'j'}\| \leq R_B]) \\ &= \sum_{s=1}^{S} \sum_{j=1}^{n_s} \min(d, N_{\boldsymbol{\mu}_{-s}}(\mu_{sj})). \end{aligned}$$

Here $N_{\boldsymbol{\mu}_{-s}}(\mu_{sj})$ is the number of between-subject neighbors that the point μ_{sj} has in the set of points $\boldsymbol{\mu}_{-s} = \{\boldsymbol{\mu}_1, \ldots, \boldsymbol{\mu}_{s-1}, \boldsymbol{\mu}_{s+1}, \ldots, \boldsymbol{\mu}_S\}$. Two points are neighbors if they are less or equal to a distance of R_B apart.

In agreement with the first stage prior (2), we specify a hard-core process for within-subject interactions. We assume that points within the same subjects have to be a minimum distance of R_W apart in order to reflect the true underlying pattern. Contrary to the first stage prior (2), however, we do not assume a constant first order term and model the between-subject interactions in (5). We discuss the method we used to specify the first order term in Section 3.1.

The second stage model (5) has parameters R_W, R_B, d, γ_B, and those used to specify $\beta(\mu)$ (see Section 3.1). We set the within-subject hard-core distance R_W to be equal to 5mm, using the same reasoning as in the case of the first stage model. The between-subject distance R_B allow us to define a spatial neighborhood. We consider points that are less than R_B apart to be connected to the same underlying functional unit in the brain. We set R_B to be equal to 5mm. This setting is motivated by our reasoning that individual units of activation should be at least 5mm apart within subjects. We set the saturation threshold d to be equal to 5.

In the second stage analysis, we are interested in inference on the between subject interaction parameter γ_B. We specify a uniform prior distribution on γ_B that with lower and upper limits 0.5 and 2, respectively. We found that this interval is wide enough to cover the range of possible values for γ_B for our data.

3.1 First order term β

We assume that the second stage point process is inhomogeneous. In the first stage analysis, we set $\beta = 1$ to allow the data Y to regulate the intensity of the point pattern in different regions of the brain. Figure 2 displays the average intensity surface $\bar{Y} = \frac{1}{n_s}\sum_{s=1}^{S} Y_s$ and the configuration of points $\boldsymbol{\mu}$ that we use as input for the second stage analysis. We see that intensity of the point

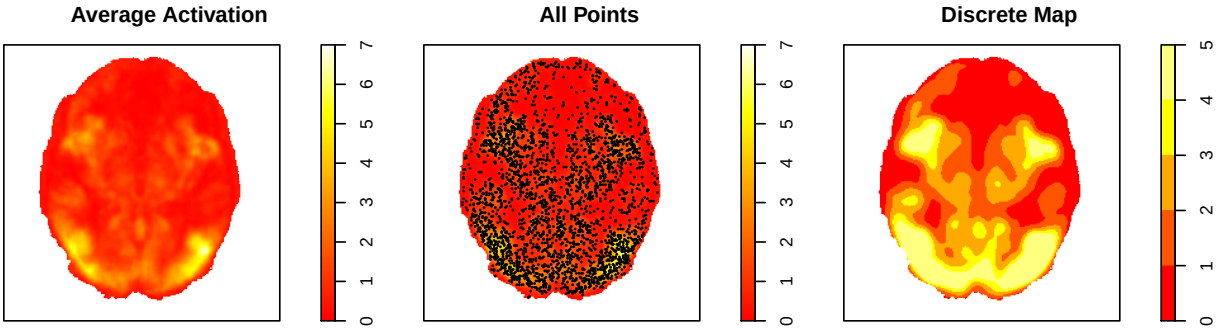

Figure 2: The average intensity surface $\bar{Y} = \frac{1}{n_s}\sum_{s=1}^{S} Y_s$ (left), the configuration of points $\boldsymbol{\mu}$ that is used input for the second stage analysis overlaid on $\bar{Y}$ (middle), and the discrete map $\bar{Y}_{1-5}$ with levels derived from $\bar{Y}$ (right).

pattern varies across the brain and that the intensity increases in areas where $\bar{Y}$ has higher values.

We considered an intensity function of the form $\beta(\mu) = \exp(\psi_1 + \psi_2\bar{Y}(\mu))$, where $\bar{Y}(\mu)$ is average surface evaluated at point μ. However, we found that this model encourages far too many points to be placed in areas where $\bar{Y}$ has high values relative to where $\bar{Y}$ has lower values. To address this issue, we transformed $\bar{Y}$ into a discrete map $\bar{Y}_{1-5}$ with levels 1 through 5 representing five areas with increasing levels of activation. The discrete map is displayed on the right hand side of Figure 2. This map reflect the changes in the intensity of the point pattern more accurately than the average map $\bar{Y}$.

We considered two forms of the intensity function based on $\bar{Y}_{1-5}(\mu)$: a) exponential $\beta(\mu) = \exp(\psi_1 + \psi_2\bar{Y}_{1-5}(\mu))$; b) and linear $\beta(\mu) = \psi_1 + \psi_2\bar{Y}_{1-5}(\mu)$. We estimated ψ_1 and ψ_2 by superimposing $\boldsymbol{\mu}_1, \ldots, \boldsymbol{\mu}_S$ onto V and fitting an inhomogeneous Poisson process model with $\bar{Y}_{1-5}$ as a covariate. We found that the linear fit accurately reflects how the intensity of points change from one region to another.

4 Markov chain Monte Carlo algorithm

In this section we describe the algorithms that we will use to sample from the posteriors $p(\boldsymbol{x}|Y)$ and $p(\gamma_B|\boldsymbol{\mu})$.

4.1 Algorithm for First Stage Model

To sample from $p(\boldsymbol{x}|Y)$ we update the configuration $\boldsymbol{x}$ at each iteration of the algorithm until convergence is reached. To update $\boldsymbol{x}$, we propose the addition, deletion or moving of a point.

Algorithm
Iterate through the following steps until convergence is reached. Set $s = 1$, and then

1. sample $r \sim \text{unif}[0,1]$

2. *if* $r \leq p_b$: propose the addition of a point to x_s
   if $p_b < r \leq (p_b + p_d)$: propose the deletion of a point of x_s
   else: propose moving a point in x_s with probability $p_m = 1 - (p_b + p_d)$

3. *if* $s = S$, end.
   else $s = s + 1$, and return to 1.[4]

For each of the birth, death, and move steps we use proposal densities q_b, q_d and q_m, respectively. Let x' denote a new configuration that is based on the current configuration x. Then, the probability with which we accept each of the steps is, respectively,

$$\begin{aligned}
\alpha_b(x, x') &= \min\left(\frac{p(x'|Y)q_d(x|x')p_d}{p(x|Y)q_b(x'|x)p_b}, 1\right) \\
\alpha_d(x, x') &= \min\left(\frac{p(x'|Y)q_b(x|x')p_b}{p(x|Y)q_d(x'|x)p_d}, 1\right) \\
\alpha_m(x, x') &= \min\left(\frac{p(x'|Y)q_m(x|x')}{p(x|Y)q_m(x'|x)}, 1\right)
\end{aligned}$$

Insertion of a point

To sample a new point $\xi = (\mu_\xi, a_\xi, d_\xi)$, we choose a proposal density function q_b that is proportional to the Papangelou conditional intensity $p(\boldsymbol{x} \cup \xi|Y)/p(\boldsymbol{x}|Y)$.

We propose the new location, height, and size parameters sequentially,

$$q_b(\boldsymbol{x} \cup \xi|\boldsymbol{x}) = q_b(\mu_\xi|a_0, d_0, \boldsymbol{x}, Y)q_b(a_\xi|\mu_\xi, d_0, \boldsymbol{x}, Y)q_b(d_\xi|\mu_\xi, a_\xi, \boldsymbol{x}, Y) \tag{6}$$

In order to propose new parameter values in turn, we use the fixed values a_0 and d_0. We set a_0 and d_0 equal to typical values of a and d, and let $a_0 = 1.5$ and $d_0 = 25\text{mm}^2$.

The birth proposal for location μ is set to be proportional to the Papangelou conditional intensity,

$$q_b(\mu_\xi|a_0, d_0, \boldsymbol{x}, Y) \propto \frac{p(\boldsymbol{\mu} \cup \mu_\xi)p(Y|\boldsymbol{x} \cup (\mu_\xi, a_0, d_0))}{p(\boldsymbol{\mu})p(Y|\boldsymbol{x})} \tag{7}$$

Here $\frac{p(\boldsymbol{\mu} \cup \mu_\xi)}{p(\boldsymbol{\mu})} = 1$ if $\|\mu_\xi - \mu_{1j}\| > R_W \ \forall j$ and zero otherwise. Assuming that the new point ξ is added to the point configuration of subject 1, the ratio of likelihoods simplify to

$$\begin{aligned}
\frac{p(Y|\boldsymbol{x} \cup (\mu_\xi, a_0, d_0))}{p(Y|\boldsymbol{x})} &= \exp[-\frac{1}{2\tau^2}\sum_v (h(v; (\mu_\xi, a_0, d_0))^2 - 2h(v; (\mu_\xi, a_0, d_0))(y_{1v} - A(v; \boldsymbol{x}_1)))] \\
&\simeq \exp[-\frac{1}{2\tau^2}(\frac{a_0^2 d_0}{2\Delta x \Delta y \log 2} - 2\sum_v h(v; (\mu_\xi, a_0, d_0))(y_{1v} - A(v; \boldsymbol{x}_1)))] \\
&\propto \exp[\frac{1}{\tau^2}(\sum_v h(v; (\mu_\xi, a_0, d_0))(y_{1v} - A(v; \boldsymbol{x}_1)))]
\end{aligned} \tag{8}$$

The above simplification is derived as follows

$$\begin{aligned}
\sum_v h(v; x_{sj})^2 \Delta x \Delta y &\simeq \int h(v; x_{sj})^2 dx dy \\
&= a_{sj}^2 d_{sj}/(2\log 2)
\end{aligned}$$

[4]Note that, instead of moving through the subjects s systematically, we can also let $s \sim \text{unif}(\{1, \ldots, S\})$.

Here Δx and Δy are the length of the voxel sides in milimeters.

To sample from (8) we need to evaluate the conditional density function at each location on the grid and use rejection sampling. The Fast Fourier Transform algorithm can be used to speed up the evaluation of (8).

To propose a height of the new point, we let

$$\begin{aligned} q_b(a_\xi|\mu_\xi, d_0, \boldsymbol{x}, Y) &\propto \frac{p(\boldsymbol{a} \cup a_\xi)p(Y|\boldsymbol{x} \cup (\mu_\xi, a_\xi, d_0))}{p(\boldsymbol{a})p(Y|\boldsymbol{x})} \\ &\propto p(a_\xi)\exp[-\frac{1}{2\tau^2}(a_\xi^2 \frac{d_0}{2\Delta x \Delta y \log 2} - 2a_\xi \sum_v h(v;\mu_\xi,1,d_0)(y_{1v} - A(v;\boldsymbol{x}_1)))] \\ &\propto p(a_\xi)p_N(a_\xi;\mu_\xi,d_0,\boldsymbol{x},Y) \end{aligned} \tag{9}$$

Here p_N is the density of a normal distribution with mean $\frac{2\Delta x \Delta y \log 2}{d_0} \sum h(v;\mu_\xi,1,d_0)(y_{1v} - A(v;\boldsymbol{x}_1))$ and variance $\frac{2\tau^2 \Delta x \Delta y \log 2}{d_0}$. We use rejection sampling to sample from (9).

We propose a value for the new size parameter based on the ratio

$$\frac{p(Y|\boldsymbol{x} \cup (\mu_\xi, a_\xi, d_\xi))}{p(Y|\boldsymbol{x})} \propto \exp[-\frac{1}{2\tau^2}(\frac{a_\xi^2 d_\xi}{2\Delta x \Delta y \log 2} - 2\sum_v h(v;(\mu_\xi,a_\xi,d_\xi))(y_{1v} - A(v;\boldsymbol{x}_1)))] \tag{10}$$

for $d_\xi \in [d_{low}, d_{up}]$. This ratio is used to derive a piecewise log-linear proposal function

$$q_b(d_\xi|\mu_\xi, a_\xi, \boldsymbol{x}, Y) \propto \exp[p_{i-1} + (p_i - p_{i-1})\frac{d_\xi - \delta_{i-1}}{\delta_i - \delta_{i-1}}] \tag{11}$$

for $d_{low} = \delta_0 < \delta_1 < \cdots < \delta_m = d_{up}$ and p_i the logarithm of ratio (10), evaluated at δ_i,

$$p_i = \log\left(\frac{p(Y|\boldsymbol{x} \cup (\mu_\xi, a_\xi, \delta_i))}{p(Y|\boldsymbol{x})}\right).$$

Removal of a point

We propose to remove point x_{sj} from the point configuration of subject s with probability $q_d(\boldsymbol{x}_{-(sj)}|\boldsymbol{x}) = 1/n_s$, for $\boldsymbol{x}_{-(sj)} = \boldsymbol{x} \setminus x_{sj}$.

Moving a point

For a move update, we randomly choose one of the n_s points of subject s. To simplify notation, let's assume that we selected point the first point of subject 1, x_{11}. Then, to obtain a good acceptance rate, we set our proposal density to be proportional to the Papangelou conditional intensity $p(\boldsymbol{x}_{-(11)} \cup \xi|Y)/p(\boldsymbol{x}_{-(11)} \cup x_{11}|Y)$. Here $\boldsymbol{x}_{-(11)}$ denotes the full point configuration $\boldsymbol{x}$ excluding point x_{11}.

Similar to the birth proposal, we update the location, height and size parameters sequentially,

$$q_m(\boldsymbol{x}_{-(11)} \cup x_\xi|\boldsymbol{x}) = q_m(\mu_\xi|a_0,d_0,\boldsymbol{x},Y)q_m(a_\xi|\mu_\xi,d_0,\boldsymbol{x},Y)q_m(d_\xi|\mu_\xi,a_\xi,\boldsymbol{x},Y)$$

We specify the proposal density for location μ to be proportional to the Papangelou conditional intensity

$$q_m(\mu_\xi|a_0,d_0,\boldsymbol{x},Y) \propto \frac{p(\boldsymbol{\mu}_{-(11)} \cup \mu_\xi)p(Y|\boldsymbol{x}_{-(11)} \cup (\mu_\xi,a_0,d_0))}{p(\boldsymbol{\mu})p(Y|\boldsymbol{x})} \tag{12}$$

Using the same steps as in the case of the birth proposal, we derive the proposal density

$$q_m(\mu_\xi|a_0,d_0,\boldsymbol{x},Y) \propto \exp[\frac{1}{\tau^2}(\sum_v h(v;\mu_\xi,a_0,d_0)(y_{1v}-A(v;\boldsymbol{x}_1\setminus x_{11})))] \quad (13)$$

if $\|\mu_\xi-\mu_{1j}\|>R_W$ for $j=2,\ldots,n_1$ and zero otherwise. As before, we use fixed values a_0 and d_0 to allow us to propose the move location, size and height in turn. We set $a_0=1.5$ and $d_0=25$.

To propose a height at the new location μ_ξ, we let

$$\begin{aligned} q_m(a_\xi|\mu_\xi,d_0,\boldsymbol{x},Y) &\propto \frac{p(\boldsymbol{a}_{-(11)}\cup a_\xi)p(Y|\boldsymbol{x}_{-(11)}\cup(\mu_\xi,a_\xi,d_0))}{p(\boldsymbol{a})p(Y|\boldsymbol{x})} \\ &\propto p(a_\xi)p_N(a_\xi;\mu_\xi,d_0,\boldsymbol{x}_1\setminus x_{11},Y) \end{aligned} \quad (14)$$

Here p_N is the density of a normal distribution with mean $\frac{2\Delta x\Delta y\log 2}{d_0}\sum h(v;\mu_\xi,1,d_0)(y_{1v}-A(v;\boldsymbol{x}_1\setminus x_{11}))$ and variance $\frac{2\tau^2\Delta x\Delta y\log 2}{d_0}$.

To propose a new value for the height parameter, we follow the same steps as for the birth update, except that p_i is now calculated as

$$\begin{aligned} p_i &= \log\left(\frac{p(Y|\boldsymbol{x}_{-(11)}\cup(\mu_\xi,a_\xi,\delta_i))}{p(Y|\boldsymbol{x})}\right) \\ &= -\frac{1}{2\tau^2}\left(\frac{a_\xi^2\delta_i}{2\Delta x\Delta y\log 2}-2\sum_v h(v;\mu_\xi,a_\xi,\delta_i)(y_{1v}-A(v;\boldsymbol{x}_1\setminus x_{11}))\right) \end{aligned}$$

4.2 Sampling from the Second Stage Model

In the second stage model, our interest is in inferring on the between-subject interaction parameter γ_B. We assume that γ_B has a informative prior on the fixed interval $[\gamma_{low},\gamma_{up}]$ Then we accept a proposed update γ_B' with probability

$$\begin{aligned} \alpha_\gamma(\gamma_B,\gamma_B') &= \min\left(\frac{p(\gamma_B'|\boldsymbol{\mu})q(\gamma_B|\gamma_B')}{p(\gamma_B|\boldsymbol{\mu})q(\gamma_B'|\gamma_B)},1\right) \\ &= \min\left(\frac{p(\gamma_B')f_{\gamma_B'}(\boldsymbol{\mu})Z_{\gamma_B}q(\gamma_B|\gamma_B')}{p(\gamma_B)f_{\gamma_B}(\boldsymbol{\mu})Z_{\gamma_B'}q(\gamma_B'|\gamma_B)},1\right) \end{aligned}$$

for second stage model $p(\boldsymbol{\mu}|\gamma_B)=f_{\gamma_B}(\boldsymbol{\mu})/Z_{\gamma_B}$ given in (5). Here $f_{\gamma_B}(\boldsymbol{\mu})$ denotes the unnormalized density function and Z_{γ_B} the intractable normalizing constant.

To avoid direct calculation of the normalizing constants, we use the auxiliary variable method proposed by Berthelsen and Møller [2006]. For this method, the authors introduced an auxilary variable $\boldsymbol{\nu}$ defined on the same state space as $\boldsymbol{\mu}$. The corresponding Hastings ratio is

$$\alpha_{\gamma,\boldsymbol{\nu}}(\gamma_B,\boldsymbol{\nu};\gamma_B',\boldsymbol{\nu}') = \min\left(\frac{p(\gamma_B',\boldsymbol{\nu}'|\boldsymbol{\mu})q(\gamma_B,\boldsymbol{\nu}|\gamma_B',\boldsymbol{\nu}')}{p(\gamma_B,\boldsymbol{\nu}|\boldsymbol{\mu})q(\gamma_B',\boldsymbol{\nu}'|\gamma_B,\boldsymbol{\nu})},1\right).$$

The proposal density for $\boldsymbol{\nu}$ and γ_B is simplified to

$$\begin{aligned} q(\boldsymbol{\nu}',\gamma_B'|\boldsymbol{\nu},\gamma_B) &= q(\gamma_B'|\boldsymbol{\nu},\gamma_B)q(\boldsymbol{\nu}'|\gamma_B',\boldsymbol{\nu}) \\ &= q(\gamma_B'|\gamma_B)q(\boldsymbol{\nu}'|\gamma_B') \end{aligned}$$

We choose the proposal density for $\boldsymbol{\nu}$ so that the normalizing constants in the Hastings ratio cancel out: $q(\boldsymbol{\nu}|\gamma_B) = f_{\gamma_B}(\boldsymbol{\nu})/Z_{\gamma_B}$. As a result the Hastings ratio simplifies to

$$\begin{aligned}
\alpha_{\gamma,\boldsymbol{\nu}}(\gamma_B, \boldsymbol{\nu}; \gamma'_B, \boldsymbol{\nu}') &= \min\left(\frac{p(\gamma'_B, \boldsymbol{\nu}'|\boldsymbol{\mu})q(\gamma_B, \boldsymbol{\nu}|\gamma'_B, \boldsymbol{\nu}')}{p(\gamma_B, \boldsymbol{\nu}|\boldsymbol{\mu})q(\gamma'_B, \boldsymbol{\nu}'|\gamma_B, \boldsymbol{\nu})}, 1\right) \\
&= \min\left(\frac{p(\gamma'_B)p(\boldsymbol{\nu}'|\gamma'_B)f_{\gamma'_B}(\boldsymbol{\mu})Z_{\gamma_B}q(\gamma_B|\gamma'_B)f_{\gamma_B}(\boldsymbol{\nu})Z_{\gamma'_B}}{p(\gamma_B)p(\boldsymbol{\nu}|\gamma_B)f_{\gamma_B}(\boldsymbol{\mu})Z_{\gamma'_B}q(\gamma'_B|\gamma_B)f_{\gamma'_B}(\boldsymbol{\nu}')Z_{\gamma_B}}, 1\right) \\
&= \min\left(\frac{p(\boldsymbol{\nu}'|\gamma'_B)f_{\gamma'_B}(\boldsymbol{\mu})q(\gamma_B|\gamma'_B)f_{\gamma_B}(\boldsymbol{\nu})}{p(\boldsymbol{\nu}|\gamma_B)f_{\gamma_B}(\boldsymbol{\mu})q(\gamma'_B|\gamma_B)f_{\gamma'_B}(\boldsymbol{\nu}')}, 1\right)
\end{aligned}$$

under the assumption that $p(\boldsymbol{\nu}, \gamma_B|\boldsymbol{\mu})$ simplifies to $p(\boldsymbol{\nu}|\gamma_B)p(\gamma_B)f_{\gamma_B}(\boldsymbol{\mu})/Z_{\gamma_B}$.

The proposal density $q(\gamma'_B|\gamma_B)$ and auxiliary density $p(\boldsymbol{\nu}|\gamma_B, \boldsymbol{\mu})$ have to be chosen to ensure good mixing properties for the algorithm. Berthelsen and Møller [2006] suggest that we let

$$p(\boldsymbol{\nu}|\gamma_B, \boldsymbol{\mu}) = f_{\bar{\gamma}_B}(\boldsymbol{\nu})/Z_{\bar{\gamma}_B} \tag{15}$$

where $\bar{\gamma}_B$ is chosen so that the posterior is concentrated around that value. We let $q(\gamma'_B|\gamma_B)$ be a Gaussian density function with mean γ_B and standard deviation equal to 0.05.

4.2.1 Generating samples from the proposal density $q(\boldsymbol{\nu}|\gamma_B)$

To implement the auxiliary variable method, we need to generate samples from model (5). We will generate samples of $\boldsymbol{\nu}$ in a similar fashion to the first stage model, in that we will iterate between the subjects, and propose the insertion, deletion or move of a point with probabilities p_b, p_d, or p_m, respectively. Then, the probability with which we accept each of the steps is, respectively,

$$\alpha_b(\boldsymbol{\nu}, \boldsymbol{\nu}') = \min\left(\frac{p(\boldsymbol{\nu}'|\boldsymbol{\mu})q_d(\boldsymbol{\nu}|\boldsymbol{\nu}')p_d}{p(\boldsymbol{\nu}|\boldsymbol{\mu})q_b(\boldsymbol{\nu}'|\boldsymbol{\nu})p_b}, 1\right) \tag{16}$$

$$\alpha_d(\boldsymbol{\nu}, \boldsymbol{\nu}') = \min\left(\frac{p(\boldsymbol{\nu}'|\boldsymbol{\mu})q_b(\boldsymbol{\nu}|\boldsymbol{\nu}')p_b}{p(\boldsymbol{\nu}|\boldsymbol{\mu})q_d(\boldsymbol{\nu}'|\boldsymbol{\nu})p_d}, 1\right) \tag{17}$$

$$\alpha_u(\boldsymbol{\nu}, \boldsymbol{\nu}') = \min\left(\frac{p(\boldsymbol{\nu}'|\boldsymbol{\mu})q_m(\boldsymbol{\nu}|\boldsymbol{\nu}')}{p(\boldsymbol{\nu}|\boldsymbol{\mu})q_m(\boldsymbol{\nu}'|\boldsymbol{\nu})}, 1\right) \tag{18}$$

$$\tag{19}$$

Insertion of a point

To add a point ν_ξ to the existing configuration, use a proposal q_b that is proportional to the Papangelou conditional intensity

$$\begin{aligned}
q_b(\nu_\xi|\boldsymbol{\nu}) &= \frac{p(\boldsymbol{\nu} \cup \nu_\xi)}{p(\boldsymbol{\nu})} \\
&= \beta(\nu_\xi)\gamma_B^{s_B(\boldsymbol{\nu}\cup\nu_\xi)-s_B(\boldsymbol{\nu})}
\end{aligned}$$

for $\|\nu_\xi - \nu_{1j}\| > R_W$ for $1 = 2, \ldots, n_1$ and zero otherwise, assuming that we propose to add point ν_ξ to the point configuration of Subject 1. Then

$$s_B(\boldsymbol{\nu} \cup \nu_\xi) - s_B(\boldsymbol{\nu}) = N_{\boldsymbol{\nu}_{-1}}(\nu_\xi) + \sum_{s=2}^{S}\sum_{j=1}^{n_s}\delta_{\boldsymbol{\nu}_{-s}\cup\nu_\xi}(\nu_{sj})$$

where

$$\delta_{\boldsymbol{\nu}_{-s}\cup\nu_\xi}(\nu_{sj}) = \begin{cases} 1 & \text{if } N_{\boldsymbol{\nu}_{-s}}(\nu_{sj}) < N_{\boldsymbol{\nu}_{-s}\cup\nu_\xi}(\nu_{sj}) \leq d, \\ 0 & \text{otherwise,} \end{cases} \tag{20}$$

Here $N_{\boldsymbol{\nu}_{-s}}(\nu_{sj})$ is the number of between-subject neighbors that the point ν_{sj} has in the set of points $\boldsymbol{\nu}_{-s} = \boldsymbol{\nu} \setminus \boldsymbol{\nu}_s$.

Deletion of a point

We propose to remove point ν_{sj} from the point configuration of subject s with probability $q_d(\boldsymbol{\nu}_{-(sj)}|\boldsymbol{\nu}) = 1/n_s$.

Moving a point

To update the location of point ν_{11}, we use a proposal q_m that is proportional to the Papangelou conditional intensity

$$\begin{aligned} q_m(\nu_\xi|\boldsymbol{\nu}) &= \frac{p(\boldsymbol{\nu}_{-(11)} \cup \nu_\xi)}{p(\boldsymbol{\nu})} \\ &= \beta(\nu_\xi)\gamma_B^{s_B(\boldsymbol{\nu}_{-(11)}\cup\nu_\xi) - s_B(\boldsymbol{\nu})} \end{aligned}$$

for $\|\nu_\xi - \nu_{1j}\| > R_W$ for $j = 2, \ldots, n_1$ and zero otherwise. Here

$$\begin{aligned} s_B(\boldsymbol{\nu}_{-(11)} \cup \nu_\xi) - s_B(\boldsymbol{\nu}) &= N_{\boldsymbol{\nu}_{-1}}(\nu_\xi) + \sum_{s=2}^{S}\sum_{j=1}^{n_s} \delta_{\boldsymbol{\nu}\setminus(\boldsymbol{\nu}_s\cup\nu_{11})\cup\nu_\xi}(\nu_{sj}) \\ &\quad - N_{\boldsymbol{\nu}_{-1}}(\nu_{11}) - \sum_{s=2}^{S}\sum_{j=1}^{n_s} \delta_{\boldsymbol{\nu}\setminus(\boldsymbol{\nu}_s\cup\nu_{11})\cup\nu_{11}}(\nu_{sj}) \end{aligned} \tag{21}$$

where

$$\delta_{\boldsymbol{\nu}\setminus(\boldsymbol{\nu}_s\cup\nu_{11})\cup\nu_\xi}(\nu_{sj}) = \begin{cases} 1 & \text{if } N_{\boldsymbol{\nu}\setminus(\boldsymbol{\nu}_s\cup\nu_{11})}(\nu_{sj}) < N_{\boldsymbol{\nu}\setminus(\boldsymbol{\nu}_s\cup\nu_{11})\cup\nu_\xi}(\nu_{sj}) \leq d, \\ 0 & \text{otherwise,} \end{cases} \tag{22}$$

Here $N_{\boldsymbol{\nu}\setminus(\boldsymbol{\nu}_s\cup\nu_{11})}(\nu_{sj})$ is the number of between-subject neighbors that the point ν_{sj} has in the set of points $\boldsymbol{\nu} \setminus (\boldsymbol{\nu}_s \cup \nu_{11})$.

4.3 Implementation

The MCMC algorithms for the first and second stage models were both implemented in R [R Core Team, 2015]. The package smoothie was used to implement the Fast Fourier Transform and packages spatstat and fields were used to generate graphs. For the first stage model, we generated a starting configuration of 4 activation units per subject (locations chosen randomly in V) and used a burn-in of $70,000$ iterations.

For the second stage model, we created a starting configuration of 3 location points per region and used a burn-in period of $20,000$ iterations. To speed up sampling from the proposal density $q(\boldsymbol{\nu}|\gamma_B)$, we first generated samples for a small set of values of γ_B, say $\gamma_{B1} < \gamma_{B2} < \cdots < \gamma_{Bm}$. Then, to generate a sample from $q(\boldsymbol{\nu}|\gamma_B)$ for $\gamma_B \in (\gamma_{Bi}, \gamma_{B,i+1})$ we use a sample from $q(\boldsymbol{\nu}|\gamma_{Bi})$ as a starting configuration.

5 Application

The model that we developed is motivated by multi-subject fMRI studies in which brain activation data is collected from a number of individuals under the same experimental conditions. As discussed in Section 1, data was collected on 21 *individuals performing an attention network test. We selected an axial slice that highlights areas that are involved in executive control function in the brain (the frontal operculum cortex and insular cortex) and in visual processing (the occipital cortex). The axial slice consist of a set of voxels with dimension* $1 \times 1 \times 1mm$ *and a* z*-statistics that reflects the strength of brain activation is calculated at each voxel location within the brain volume.*

We fitted our first stage model to the maps of z-statistics to identify a configuration of activation units for each individual. We applied our MCMC algorithm described above, using the parameter and hyperparameter settings discussed in Section 2.3. In Figure 3 we display the fitted activation surface along with the true surface for the same four individuals as in Figure 1. We see that there is a fair amount of subject to subject variability in the activation surfaces

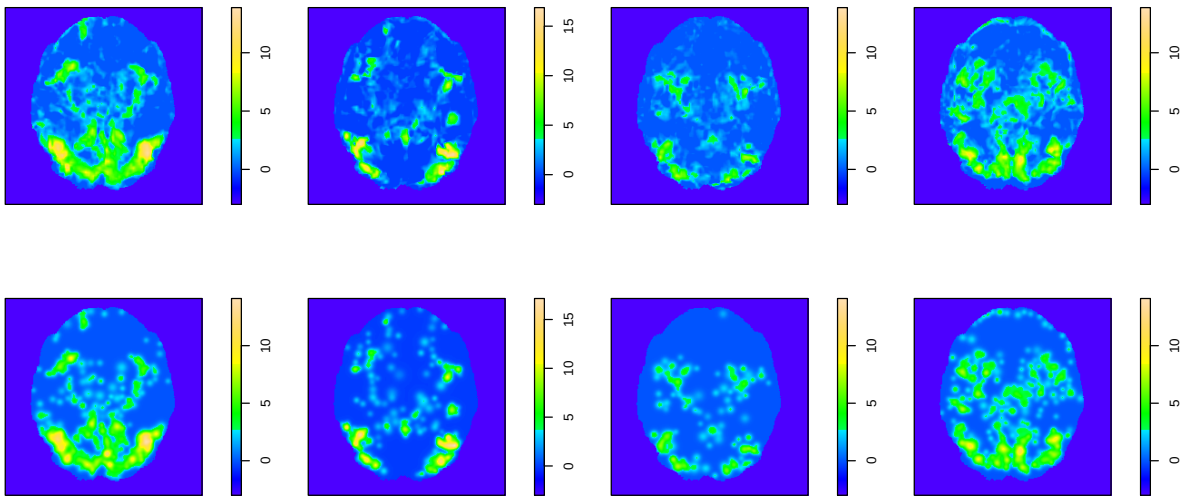

Figure 3: The activation surfaces (top row) and corresponding fitted surfaces $A_s = A(v; \boldsymbol{x}_s | v \in V)$ (bottom row) of four of the subjects for the selected axial slice.

in terms of the spatial extent and amplitude of activation. Visual inspection suggests that the model does well picking up regions of activation.

Table 1 gives a summary of the configuration of activation units fitted for each subject. We calculate the summary measures at the subject level and report the corresponding mean and standard deviations of these measures. In addition, we report the mean maximum height $\max(Y_{sv} | v \in V)$ and its standard deviation. We see that the number of activation units fitted can vary greatly from subject to subject, allowing the first stage model to accurately reflect the between-subject variability in the spatial extent of activated areas as observed in Figure 3. We also note that the high within-subject variability in the height and size parameters, indicating that the model is able to describe small activation regions with low amplitude as well as spatially extended activation regions with high amplitude.

For the second stage analysis, we used the configuration of activation locations $\boldsymbol{\mu}$ that

Measure	Mean	St. Dev. (between)	Mean St. Dev. (within)
n_s	137.29	36.02	
$\frac{1}{n_s}\sum_{j=1}^{n_s} a_{sj}$	3.02	0.46	1.58
$\frac{1}{n_s}\sum_{j=1}^{n_s} d_{sj}$	38.74	2.89	16.47
$\frac{1}{n_s}\sum_{j=1}^{n_s}(Y_{sv} - A(v;\boldsymbol{x}_s))^2$	0.24	0.09	
$\max(Y_{sv}\|v \in V)$	9.70	3.19	

Table 1: Summary measures for the configuration of activation units of the first stage model and the maximum height of the activation surface Y. The following summary measures are calculated: number of units per subject, the average height and size of the activation units, and the mean square error. The summary measures are calculated at the subject level and the corresponding means and standard deviations of these summaries are reported. For the height and size parameters, we also report the average within-subject standard deviation.

maximized the first stage posterior distribution as input. Our goal with this analysis is to get insight into the inter-subject patterns of clustering that we observe in different functional areas of the brain. We identified four functional areas of interest which we label Regions 1 through 4. These regions are indicated on the axial slice in Figure 4. Regions 1 and 2 correspond to the left

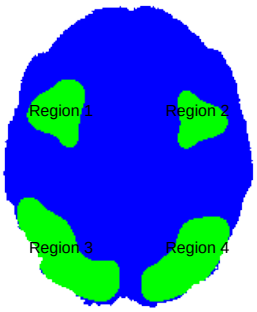

Figure 4: The four regions of brain activation identified for the second stage analysis.

and right frontal operculum and insular cortices, respectively, and Regions 3 and 4 correspond to the left and right inferior lateral occipital cortex.

We hypothesize that we will observe patterns of clustering in brain areas that engage in the experimental tasks. However, we would like to investigate whether the degree or strength of clustering vary among the regions. We report the posterior mean of the inter-subject interaction parameter γ_B in Table 2 for each of the four regions and for the background region (the area that is indicated in blue in Figure 4), and we find that the highest degree of inter-subject clustering occurs in Region 2.

We fitted our second stage model using the MCMC algorithm described in Section 4.2. The parameter settings for this model was discussed and motivated in Section 3. When implementing our MCMC algorithm to sample γ_B in each of the four regions, we found that several points in the simulated configurations $\boldsymbol{\nu}$ lie close to or on the boundaries of these regions. To get

Region	Mean	St. Dev.
Region 1 (left operculum and insular cortices)	1.33	0.005
Region 2 (right operculum and insular cortices)	1.41	0.006
Region 3 (left occipital cortex)	1.26	0.005
Region 4 (right occipital cortex)	1.25	0.005
Background	1.10	0.002

Table 2: The posterior mean and standard deviation of the mean of the inter-subject interaction parameter γ_B for each of the four regions and the background region.

an accurate count of the number of neighbors of these points, we created a boundary region for each of Regions 1 through 4. These regions are at least 5 voxels wide. Point processes $\boldsymbol{\nu}$ were then simulated on the expanded regions (orginal region plus boundary region), and the simulated points in the boundary regions were used to ensure an accurate neighbor count for points in Regions 1 through 4.

6 Discussion

In this paper we developed a new approach for analyzing multi-subject fMRI data. Our approach is based on using a two stage spatial point process model that first identify the image elements of interest and then study the interactions among these elements.

The two stage point process model that we developed is motivated by the unique features of multi-subject fMRI data. First, we do not observe the point pattern data directly. Second, the data is collected for several subjects under the same experimental conditions on a study area (grid of voxels) V, and, finally, we assume that the subject data has been spatially aligned on V (*i.e.* a specific voxel location matches to the same functional area for all the subjects). With these features in mind, we developed a model that gives us insight into how information about activation is shared across subjects in different functional regions of the brain.

For the first stage analysis, we proposed a marked spatial point process model to allow us to identify individual units of activation for each of the subjects in our study. These activation units summarize the activation patterns that we observe for the selected axial slice in the brain volume. The marked spatial point process prior model enforces a set of constraints on the activation units. One of these constraints is that the units should be at least some minimal distance apart within subjects. We use this distance constraint to define a spatial neighborhood. Points that are less than this distance apart are assumed to be connected to the same underlying functional in the brain.

Our second stage model is designed to give us insight into how information is shared across subjects. We developed a pairwise interaction model that counts the number of inter-subject points that are within the same spatial neighborhood. By studying the degree of clustering, we can learn about about how activation varies in different parts of the brain that are connected to the experimental conditions under study.

We reported the results of fitting our two-stage model to data from an fMRI study in which subjects were asked to perform an attention network test. We found that our first stage model did well in describing the activation patterns of the 21 *subjects in our study. For the second stage analysis, we used as input the configuration of activation locations that maximized the first stage posterior. We identified four functional regions in the brain are involved in the attention*

network task: the left and right frontal operculum and insular cortices, and the left and right inferior lateral occipital cortex. The operculum and insular cortices are involved in executive control function in the brain and the occipital cortex in visual processing.

We hypothesized that we would observe patterns of inter-subject clustering in brain areas that engage in the experimental tasks, and found that the frontal operculum and insular cortices show a higher degrees of clustering relative to the occipital cortex. We observed the highest degree of clustering in the right frontal operculum and insular cortices. A possible explanation for this pattern is that the right insular lesions have more of a role in multisensory integration. The right anterior insula is also posited to have a role in network switching (recruiting the dorsal attention network that would respond to the target).

Although we do not explore this further here, our first stage analysis model can also be used to provide summaries in terms of height, size and location of activation in order to compare activation in different parts of the brain or to compare activation for different groups of individuals. These insights are hard to come by with traditional voxel-by-voxel analysis models. In addition, the configuration of activation units can also be used as input to methods that calculate the probability of activation at each voxel location or that classify voxels as activated or not activated.

In summary, the model that we introduce in this paper allows us to study how information about activation is shared in different functional areas in the brain. For the purposes of our analysis, we only considered information sharing within the same underlying functional area. Our model can be extended to include longer-range interactions and to study how different functional areas interact with each other.

References

Fahimah Al-Awadhi, Merrilee Hurn, and Christopher Jennison. Three-dimensional bayesian image analysis and confocal microscopy. *Journal of Applied Statistics*, 38(1):29–46, 2011.

Adrian J Baddeley and MNM Van Lieshout. Area-interaction point processes. *Annals of the Institute of Statistical Mathematics*, 47(4):601–619, 1995.

AJ Baddeley and MNM Van Lieshout. Stochastic geometry models in high-level vision. *Journal of Applied Statistics*, 20(5-6):231–256, 1993.

Christian F Beckmann, Mark Jenkinson, and Stephen M Smith. General multilevel linear modeling for group analysis in fmri. *Neuroimage*, 20(2):1052–1063, 2003.

Kasper K. Berthelsen and Jesper Møller. Bayesian analysis of markov point processes. In *Case Studies in Spatial Point Process Modeling*, pages 85–97. Springer, 2006.

Peter J Diggle, Jorge Mateu, Helen E Clough, et al. A comparison between parametric and non-parametric approaches to the analysis of replicated spatial point patterns. *Advances in Applied Probability*, 32(2):331–343, 2000.

Peter J Diggle, Stephen J Eglen, and John B Troy. Modelling the bivariate spatial distribution of amacrine cells. In *Case Studies in Spatial Point Process Modeling*, pages 215–233. Springer, 2006.

Stefanie Eckel, Frank Fleischer, Pavel Grabarnik, Marian Kazda, Aila Särkkä, and Volker Schmidt. Modelling tree roots in mixed forest stands by inhomogeneous marked gibbs point processes. *Biometrical Journal*, 51(3):522–539, 2009.

Jin Fan, Bruce D McCandliss, John Fossella, Jonathan I Flombaum, and Michael I Posner. The activation of attentional networks. *NeuroImage*, 26(2):471–479, 2005.

Karl J Friston, Daniel E Glaser, Richard NA Henson, S Kiebel, Christophe Phillips, and John Ashburner. Classical and bayesian inference in neuroimaging: applications. *Neuroimage*, 16 (2):484–512, 2002a.

Karl J Friston, William Penny, Christophe Phillips, S Kiebel, G Hinton, and John Ashburner. Classical and bayesian inference in neuroimaging: theory. *NeuroImage*, 16(2):465–483, 2002b.

CJ Geyer. Likelihood inferentce for spatial point processes. In OE Barndorff-Nielson, WS Kendall, and MNM van Lieshout, editors, *Stochastic geometry: likelihood and computation*. Chapman & Hall, Boca Raton, 1999.

Pavel Grabarnik and Aila Särkkä. Interacting neighbour point processes: some models for clustering. *Journal of Statistical Computation and Simulation*, 68(2):103–125, 2001.

Niels Væver Hartvig. A stochastic geometry model for functional magnetic resonance images. *Scandinavian Journal of Statistics*, 29(3):333–353, 2002.

Mark Jenkinson, Christian F Beckmann, Timothy EJ Behrens, Mark W Woolrich, and Stephen M Smith. FSL. *NeuroImage*, 62(2):782–790, 2012.

Jian Kang, Timothy D Johnson, Thomas E Nichols, and Tor D Wager. Meta analysis of functional neuroimaging data via bayesian spatial point processes. *Journal of the American Statistical Association*, 106(493):124–134, 2011.

Seyoung Kim, Padhraic Smyth, and Hal Stern. A bayesian mixture approach to modeling spatial activation patterns in multisite fmri data. *Medical Imaging, IEEE Transactions on*, 29(6):1260–1274, 2010.

Tara M Madhyastha, Mary K Askren, Peter Boord, and Thomas J Grabowski. Dynamic connectivity at rest predicts attention task performance. *Brain connectivity*, 5(1):45–59, 2015.

Jesper Møller. Markov chain monte carlo and spatial point processes. In OE Barndorff-Nielson, WS Kendall, and MNM van Lieshout, editors, *Stochastic geometry: likelihood and computation*. Chapman & Hall, Boca Raton, 1999.

Mari Myllymäki, IG Panoutsopoulou, and Aila Särkkä. Analysis of spatial structure of epidermal nerve entry point patterns based on replicated data. *Journal of microscopy*, 247(3): 228–239, 2012.

Thomas E Nichols and Andrew P Holmes. Nonparametric permutation tests for functional neuroimaging: a primer with examples. *Human brain mapping*, 15(1):1–25, 2002.

R Core Team. *R: A Language and Environment for Statistical Computing*. R Foundation for Statistical Computing, Vienna, Austria, 2015. URL `http://www.R-project.org/`.

Katja Schladitz, Aila Särkkä, Iris Pavenstädt, Otto Haferkamp, and Torsten Mattfeldt. Statistical analysis of intramembranous particles using freeze fracture specimens. *Journal of microscopy*, 211(2):137–153, 2003.

Lance A Waller, Aila Särkkä, Viktor Olsbo, Mari Myllymäki, Ioanna G Panoutsopoulou, William R Kennedy, and Gwen Wendelschafer-Crabb. Second-order spatial analysis of epidermal nerve fibers. *Statistics in Medicine*, 30(23):2827–2841, 2011.

Wouter D Weeda, Lourens J Waldorp, Ingrid Christoffels, and Hilde M Huizenga. Activated region fitting: A robust high-power method for fmri analysis using parameterized regions of activation. *Human brain mapping*, 30(8):2595–2605, 2009.

Mark W Woolrich, Timothy EJ Behrens, Christian F Beckmann, Mark Jenkinson, and Stephen M Smith. Multilevel linear modelling for fmri group analysis using bayesian inference. *Neuroimage*, 21(4):1732–1747, 2004.

Keith J Worsley, CH Liao, J Aston, V Petre, GH Duncan, F Morales, and AC Evans. A general statistical analysis for fmri data. *Neuroimage*, 15(1):1–15, 2002.

Lei Xu, Timothy D Johnson, Thomas E Nichols, and Derek E Nee. Modeling inter-subject variability in fmri activation location: A bayesian hierarchical spatial model. *Biometrics*, 65 (4):1041–1051, 2009.